JCTC Journal of Chemical Theory and Computation

pubs.acs.org/JCTC Article

Variational Squeezed Davydov Ansatz for Realistic Chemical Systems with Nonlinear Vibronic Coupling

Jiarui Zeng and Yao Yao*

Cite This: J. Chem. Theory Comput. 2022, 18, 1255−1263 Read Online

ACCESS | Metrics & More | Article Recommendations | Supporting Information

ABSTRACT: Chemical systems normally possess strong nonlinear vibronic couplings at both zero and finite temperature. For the lowest-order quadratic couplings, here, we introduce a squeezing operator into a variational coherent-state-based method, Davydov ansatz, to simulate the quantum dynamics and the respective spectroscopy. Two molecular systems, pyrazine and the 2-pyridone dimer, are taken as calculated model systems, both of which involve nontrivial quadratic vibronic couplings in high- and low-frequency regions, respectively. Upon a comparison with the benchmarks, the method manifests its advantage for nonlinear couplings. The squeezed bases are also proven to be applicable for the finite temperature by adapting with the thermofield dynamics.

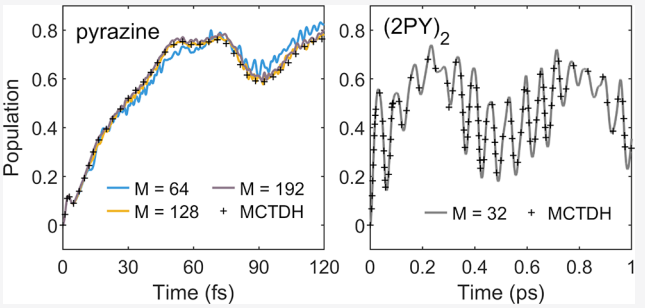

1. INTRODUCTION

Nuclear vibration is considered to have a significant role in organic optoelectronic materials due to ubiquitous vibronic coupling to electronic states.[1] Such a regime gives rise to a breakdown of the Born−Oppenheimer approximation, and one would obtain a comprehensive picture from a perspective of nonadiabatic dynamics.[2,3] Therefore, it is important to find an approach to capture the essential physics, which can help with the physical and chemical manipulations such as temperature or substitution to achieve an expected feature.[4,5] To describe the potential energy surfaces (PES), the vibronic coupling model was proposed as an efficient approach and has been successfully employed in a large number of molecular systems.[1,6−10] In this model, electronic states are modeled as a diabatic representation, and the vibronic couplings are decomposed into low-order couplings in a Taylor series. The linear vibronic coupling has been well-studied and can cause the conical intersection (CI) of the PES and lead to a radiationless electronic transition in the photodynamics.[11,12] Moreover, the quadratic and bilinear vibronic couplings have also attracted increasing attention recently.[8,10,13,14] These couplings occur in the change of vibrational frequency, Duschinsky effect, or bilinear interstate coupling.[13] It has been found that the quadratic coupling can complicate the PES and significantly influence the quantum dynamics and spectroscopy such as in thymine.[13]

It remains a nontrivial problem to describe the quantum dynamics of the vibronic coupling model, because of the difficulties of tackling a sophisticated system in an analytical framework.[15] In order to solve the time-dependent Schrödinger equation, many quantum dynamics methods with different strategies have been proposed over the past several decades. For example, the multiconfigurational time-dependent Hartree (MCTDH) method and the time-dependent density matrix renormalization group (tDMRG) method generally use bosonic number states to represent the vibration and are able to provide accurate simulations.[16−22] In order to avoid the exponential computational cost with the increasing dimension of the Hilbert space, a decomposition is necessary to reduce the high-order tensor.[16,17,20,23] Another way is to describe the vibration as a bath and focus on the reduced density matrix of the remaining part. The master equation methods are known as the Redfield equation and the hierarchical equations of motion (HEOM).[24−26]

An alternative approach is to utilize a representation of coherent states.[27] The Davydov ansatz method mimics each vibrational mode with a coherent state instead of using the bosonic number state, and the Dirac−Frenkel variational principle is employed in order to determine its time-dependent parameters.[28] The Davydov ansatz with localized coherent-state representation (D_1 ansatz) has become an efficient tool such as in the spin-boson model and the singlet fission.[29,30] To improve the computational performances, there are also extensions developed on the basis of this method. For example, based on the D_2 ansatz, which has a delocalized coherent-state representation, Werther and Grossmann biased

Received: August 25, 2021
Published: January 31, 2022

https://doi.org/10.1021/acs.jctc.1c00859
J. Chem. Theory Comput. 2022, 18, 1255−1263

the variational parameters of the coherent states and used the Bargmann coherent state to reduce the dimension of the linear differential equations.[31] This method has an intermediate performance between the D_1 and D_2 ansatz.[31,32] On the other hand, when the complicated and strong quadratic couplings are considered in the model, a tailored method would be able to grasp more dynamics features in computational simulations, that is, to introduce a squeezing operator into the ansatz, which is expected to adjust the Hilbert space to be more appropriate for the description with the coherent states. The squeezing operator was first adopted into the D_1 ansatz by Grossmann et al.[33] to calculate the spin-boson model. It was also applied to the D_2 ansatz to discuss the shift effect of vibrational frequencies and describe the Morse oscillators.[34,35] A similar strategy was also applied in the Gauss−Hermite basis method, which introduces a Hermite polynomial to a Gaussian wave function and was employed to calculate the semiclassical and/or nonadiabatic dynamics.[36−39] In addition, the generalized Gauss−Hermite basis, also known as the generalized coherent state in the quantum optics literature, was developed with a fully variational methodology for the molecular and spin-boson dynamics.[40−42]

However, both the D_1 and D_2 ansatz and their squeezed variants are hard to employ in realistic chemical systems. It is difficult for the D_1 ansatz to provide a good description of the off-diagonal coupling while it is very common in the vibronic coupling model.[43] On the other hand, the D_2 ansatz could not even reflect the decoherence of the electronic density matrix, which is inevitable while considering the finite temperature. Recently, the multiple Davydov ansatz has been developed. Constructed with a superposition of the single Davydov ansatz, this method (including the multi-D_1 and multi-D_2 ansatz) allows a description of the transition between different potential traps and has become a powerful tool for both diagonal and off-diagonal coupling schemes in numbers of chemical and physical domains.[43−46] In this work, we introduce the squeezing operator into the multi-D_2 ansatz, namely, the multi-S_2 ansatz, to simulate realistic chemical systems while involving the quadratic vibronic coupling. Accordingly, the representation of the vibration becomes a direct product of the coherent states and the squeezed states, and both of them are determined by the variational principle. In order to exhibit the performance of the multi-S_2 ansatz, two realistic chemical molecules are simulated and compared with the benchmark results of the MCTDH method. Moreover, the finite temperature is taken into account to investigate its influence using the thermofield dynamics (TFD) method.[47,48] This method was introduced to calculate the electron-vibrational Hamiltonian by Borrelli and Gelin and was shown to be able to circumvent multiple sampling calculations to obtain the statistical average of observables.[49] In addition, recently, Borrelli and Gelin combined the TFD methods with the tensor-train (TT) method, clearly demonstrating and exhibiting its potential for numerically accurate simulations of linear and nonlinear spectroscopy as well as quantum dynamics.[50−54] As a highly promising method, it was also applied in the Davydov ansatz to investigate the finite temperature effect.[55]

The rest of the paper is organized as follows. In Section 2, we describe the general vibronic coupling model, the TFD method, and the multi-S_2 ansatz as well as relevant observables involved in our simulations. Considering two kinds of molecules, the pyrazine and the 2-pyridone dimer, we exhibit their simulation results and discuss them in Sections 3.1 and 3.2, respectively. Finally, a conclusion is given in Section 4.

2. HAMILTONIAN AND METHODOLOGY

In this section, the model Hamiltonian, the TFD method, and the multi-S_2 ansatz as well as observables of interest are briefly described. The Supporting Information is accessible for detailed derivations. For a realistic molecular system, considering two electronic states, the vibrations of nuclei, and their vibronic couplings, the model Hamiltonian can be written as

$$H = \begin{pmatrix} \epsilon_1 & 0 \\ 0 & \epsilon_2 \end{pmatrix} + \sum_q \omega_q b_q^\dagger b_q + \sum_q \begin{pmatrix} a_q & c_q \\ c_q & b_q \end{pmatrix} (b_q^\dagger + b_q) + \sum_{p,q} \begin{pmatrix} a_{pq} & c_{pq} \\ c_{pq} & b_{pq} \end{pmatrix} (b_p^\dagger + b_p)(b_q^\dagger + b_q) \tag{1}$$

Herein, the first term represents diabatic electronic states with energies ϵ_1 and ϵ_2. $b_q^\dagger$ (b_q) is the creation (annihilation) operator of the qth vibrational mode with a frequency of ω_q. The third and last terms are truncations of the vibronic couplings in a Taylor series, leading to linear vibronic couplings and quadratic/bilinear vibronic couplings, respectively. In this work, simulations referring to the LVC model consider only the linear couplings in the Hamiltonian. If both types of couplings are included, the model Hamiltonian is labeled as the QVC model.

Solving the time-dependent Schrödinger equation with H, one can obtain the wave packet propagation at zero temperature. In order to perform the simulations at finite temperature, the TFD method is adopted in our work. The statistical average of observables in the framework of the TFD is described by a modified Hamiltonian containing real and fictitious parts:[47,49]

$$\hat{H} = H - \tilde{H} \tag{2}$$

where the fictitious part $\tilde{H}$ can be derived from H and acts on the fictitious states. Then, the TFD Schrödinger equation can be written as

$$i\frac{\partial}{\partial t}|\psi(t)\rangle = \hat{H}|\psi(t)\rangle \tag{3}$$

Herein, the wave function

$$|\psi(t)\rangle = \rho(t)^{1/2}|\mathbf{I}\rangle = \sum_n \rho(t)^{1/2}|n\tilde{n}\rangle \tag{4}$$

containing both real basis vectors $|n\rangle$ and fictitious basis vectors $|\tilde{n}\rangle$. $\rho(t)$ is the density matrix of the system. Assuming the system evolves from the thermal equilibrium at a given temperature T, the initial condition can be written as

$$|\psi(0)\rangle = \rho(0)^{1/2}|\mathbf{I}\rangle = Z^{-1/2}e^{-\beta H/2}|\mathbf{I}\rangle \tag{5}$$

where $Z = \mathrm{Tr}[e^{-\beta H}]$ and $\beta = 1/k_B T$. k_B is the Boltzmann constant. Then, we are able to obtain the expectation of an observable A with eq 5

$$\langle A\rangle = \mathrm{Tr}[\rho(0)A] = Z^{-1}\sum_n \langle n|A|n\rangle e^{-\beta E_n} \tag{6}$$

and its time-dependent version

https://doi.org/10.1021/acs.jctc.1c00859
J. Chem. Theory Comput. 2022, 18, 1255−1263

$$\langle A(t)\rangle = \mathrm{Tr}[\rho(t)A] \tag{7}$$

Following Borrelli and Gelin, the electronic energy difference is assumed to be larger than 0.026 eV which corresponds to room temperature.[49] Therefore, the electronic subsystem would be less influenced at finite temperature, and all of the fictitious terms referring to the electronic part can be dropped. Furthermore, the system is assumed to be factorized. Then, the Hamiltonian and the initial wave function can be written as

$$\tilde{H} = \sum_q \omega_q \tilde{b}_q^\dagger \tilde{b}_q \tag{8}$$

and

$$|\psi(0)\rangle = |e\rangle\rho_{\mathrm{vib}}^{1/2}|\mathbf{I}\rangle \tag{9}$$

where $|e\rangle$ is the initial electronic state. In this case, eq 9 can be equivalently written as a Bogoliubov transformation acting on the vibrational vacuum state:[56]

$$\rho_{\mathrm{vib}}^{1/2}|\mathbf{I}\rangle = e^{-iG}|\mathbf{0}\rangle \tag{10}$$

where

$$G = -i\sum_q \theta_q(b_q\tilde{b}_q - b_q^\dagger\tilde{b}_q^\dagger) \tag{11}$$

with

$$\theta_q = \mathrm{arctanh}(e^{-\beta\omega_q/2}) \tag{12}$$

and $|\mathbf{0}\rangle = |0\tilde{0}\rangle$.

Instead of solving eq 3 with the initial condition eq 9, it is more convenient to make the Bogoliubov operator act on $\hat{H}$, and finally, we solve the TFD Schrödinger equation with an initial condition $|\varphi(0)\rangle = |e\rangle|\mathbf{0}\rangle$ and a Hamiltonian which can be written as

$$\begin{aligned}\bar{H} = {} & \begin{pmatrix}\epsilon_1 & 0\\ 0 & \epsilon_2\end{pmatrix} + \sum_q \omega_q(b_q^\dagger b_q - \tilde{b}_q^\dagger\tilde{b}_q) + \sum_q \begin{pmatrix}a_q & c_q\\ c_q & b_q\end{pmatrix}[\cosh\theta_q(b_q^\dagger + b_q)\\ & + \sinh\theta_q(\tilde{b}_q^\dagger + \tilde{b}_q)] + \sum_{p,q}\begin{pmatrix}a_{pq} & c_{pq}\\ c_{pq} & b_{pq}\end{pmatrix}[\cosh\theta_p(b_p^\dagger + b_p)\\ & + \sinh\theta_p(\tilde{b}_p^\dagger + \tilde{b}_p)][\cosh\theta_q(b_q^\dagger + b_q) + \sinh\theta_q(\tilde{b}_q^\dagger + \tilde{b}_q)]\end{aligned} \tag{13}$$

It can be seen the quadratic couplings change as a square of a hyperbolic function, leading to a more rapid increase than the linear couplings for those low frequencies. Therefore, while considering the strong quadratic vibronic couplings or the low-frequency couplings at finite temperature, it should be carefully treated with a more tailored method. In this work, the multi-S_2 ansatz is adopted which has the expression of a squeezing operator acting on the multi-D_2 ansatz:

$$|S_2(t)\rangle = S(t)|D_2(t)\rangle \tag{14}$$

where

$$\begin{aligned}|D_2(t)\rangle = {} & \sum_i^M (A_i(t)|1\rangle + B_i(t)|2\rangle)\\ & \otimes \exp\left(\sum_q \beta_{iq}(t)b_q^\dagger - \beta_{iq}^*(t)b_q\right)|0\rangle_{\mathrm{ph}}\end{aligned} \tag{15}$$

and

$$S(t) = \exp\left(\frac{1}{2}\sum_q \zeta_q(t)b_q^{\dagger 2} - \zeta_q^*(t)b_q^2\right) \tag{16}$$

Herein, A_i/B_i, β_{iq}, and ζ_q are the variational parameters of the electronic states, the coherent states, and the squeezed states, respectively. M is the multiplicity of the multi-S_2 ansatz. The squeezing operator can also be regarded as a kind of Bogoliubov operator, and it has the following properties:

$$\hat{S}^\dagger b_q \hat{S} = b_q\,\mathrm{cosh}|\zeta_q| + b_q^\dagger e^{i\theta_q}\,\mathrm{sinh}|\zeta_q| \tag{17}$$

and

$$\hat{S}^\dagger b_q^\dagger \hat{S} = b_q^\dagger\,\cosh|\zeta_q| + b_q e^{-i\theta_q}\sinh|\zeta_q| \tag{18}$$

with $\zeta_q = |\zeta_q|e^{i\theta_q}$. Therefore, it is expected to adjust the Hamiltonian, especially the nonlinear terms in wave packet propagation, leading to a more "linear" Hilbert space for the description with the coherent state. To determine the variational parameters in the propagation, we utilize the Dirac–Frenkel time-dependent variational principle which can be written as[29]

$$\delta\int_0^t L\,\mathrm{d}t = 0 \tag{19}$$

where the Lagrangian L is defined as

$$L = \langle S_2(t)|\left(\frac{i}{2}\overrightarrow{\partial_t} - \frac{i}{2}\overleftarrow{\partial_t} - H\right)|S_2(t)\rangle \tag{20}$$

Using eq 19, one can obtain equations of motion for a variational parameter u which can be A_i, B_i, β_{iq}, or ζ_q:

$$\frac{\mathrm{d}}{\mathrm{d}t}\frac{\partial L}{\partial \dot{u}^*} - \frac{\partial L}{\partial u^*} = 0 \tag{21}$$

For a factorized initial condition, variational parameters except $A_1(0)$ and $B_1(0)$ are set as zero. That is, $A_i(0)/B_i(0)$ ($i > 1$), $\beta_{iq}(0)$, and ζ_q (0) (i from 1 to M, q for all vibrational modes) are set as zero. However, in our practical calculations, when the rigorous zero values are applied to the variational parameters, the singularity in solving the linear equations will be confronted. To avoid this problem, we add the initial random noise of $|\varepsilon_e| < 10^{-3}$, $|\varepsilon_c| < 1$, and $|\varepsilon_s| < 10^{-6}$ onto $A_i(0)/B_i(0)$, $\beta_{iq}(0)$, and $\zeta_q(0)$ ($i > 1$), respectively.

After obtaining the propagation of the wave function, some observables are calculated for a comparison with the benchmarks and an investigation of features. First, we calculate the diabatic population of electronic states. Considering the definition of the multi-S_2 ansatz, the population of the first electronic state can be written as

$$P(t) = \sum_{ji} A_j^*(t)\,A_i(t)R_{ji} \tag{22}$$

Herein, the squeezing operator is canceled in the formula, and R_{ji} is the Debye–Waller factor defined as

$$R_{ji} = \exp\left(\sum_q \beta_{jq}^*(t)\,\beta_{iq}(t) - \frac{|\beta_{jq}(t)|^2 + |\beta_{iq}(t)|^2}{2}\right) \tag{23}$$

Another physical quantity of interest is the spectrum intensity, which can be calculated by the Fourier transformation of the autocorrelation function as follows:

https://doi.org/10.1021/acs.jctc.1c00859
J. Chem. Theory Comput. 2022, 18, 1255−1263

$$I(\omega) = \int C(t)e^{i\omega t}\,dt \tag{24}$$

with

$$C(t) = \langle S_2^*(t/2)|S_2(t/2)\rangle \tag{25}$$

$C(t)$ is called the autocorrelation function which is the overlap between the initial and final state, and it is used to describe the coherence of the system. In the experimental spectrum, lines are broadened due to the resolution of the spectrometer.[7] To reproduce this effect, a damping curve $h(t) = e^{-t/\tau}$ is multiplied to the autocorrelation function, where τ is a phenomenological damping parameter determining the broadening of the spectrum.

3. NUMERICAL RESULTS

In this section, two molecular systems are calculated: the pyrazine model describing the photodynamics after excitation from the ground state onto the $\pi\pi^*$ state, and the vibronic coupling system in hydrogen-bonded 2-pyridone dimer describing the vibronic spectroscopy and the excitonic transfer.

3.1. Pyrazine. To examine the performance of the multi-S_2 ansatz, we calculate the pyrazine model containing the lowest two excited electronic states. In such a molecule, vibrational modes with the four strongest vibronic couplings lead to ultrafast radiationless decay processes through the CI, and other bathlike ones manifest a reducing effect in the absorption spectrum.[7] Two kinds of pyrazine models are adopted from refs 7 and 8. The former only considers the linear couplings, but it is not the true model for the pyrazine. The latter models the vibrational modes extending to quadratic and bilinear terms and meets the correct features. Both LVC and QVC models are challenging for simulations and have been used as criteria to test the efficiency of the quantum dynamics methods.[22,39,45,57,58] First, we calculate two reduced-dimension Hamiltonians involving vibrational modes ν_{6a}, ν_1, ν_{9a}, and ν_{10a}, namely, the reduced LVC and reduced QVC model. Corresponding results of a diabatic population are illustrated in Figure 1a,b, in which benchmark results for comparison are also calculated using the Heidelberg MCTDH package.[59] It can be seen in the case of small multiplicity that populations are fluctuated and less accurate. The feature of fluctuation is related to the initial random noise of the variational parameters, and lines become smoother and nearly coincide with the MCTDH results as the multiplicity increases. This shows the effectiveness of the multi-S_2 ansatz for both cases of linear couplings and mixed linear/bilinear couplings.

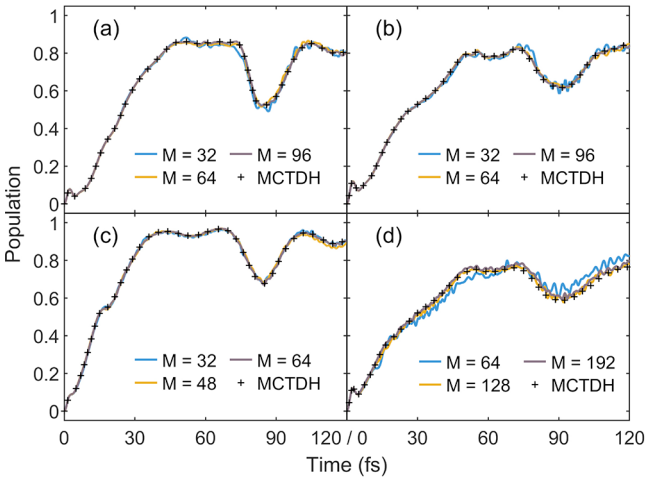

Figure 1. Diabatic population of the $n\pi^*$ state of pyrazine with (a) the reduced LVC model, (b) the reduced QVC model, (c) the full-modes LVC model, and (d) the full-modes QVC model. Solid lines are calculated via the multi-S_2 ansatz with different multiplicities, and dotted lines are the MCTDH results.

Then, we calculate the population dynamics with full modes in Figure 1c,d. It should be mentioned that, for the QVC model, when the strong bilinear coupling $b_{18b,19b}$ is applied to the multi-S_2 ansatz, simulations require a gradually decreasing step size when the wave packet propagates. In the linear-coupling scheme, when the bathlike vibrational modes are included in the Hamiltonian, the multiplicity becomes less demanding, and it yields a consistent result even with $M = 32$. This feature can be explained by the dedamping effect which has been discussed by Chen et al.[45] However, it becomes different when the second-order interactions are involved. Although the multi-S_2 ansatz with $M = 64$ can obtain a converged result for the reduced Hamiltonian, deviation and fluctuation can be recognized when the method is employed to the full-modes one. As the multiplicity increases to $M = 128$, a good result approaching the benchmark can be obtained. As a consequence, the multi-S_2 ansatz manifests its ability to provide a reliable simulation in the population dynamics for realistic chemical systems such as pyrazine.

For the full-modes QVC Hamiltonian, we adjust the bilinear coupling $b_{18b,19b}$ to the CASSCF value of 0.001 45 eV and employ a much larger step size, which allows us to propagate the wave packet in a longer time scale and with a larger multiplicity.[8] In this case, the diabatic population is again calculated to compare with the multi-D_2 ansatz in Figure 2. It

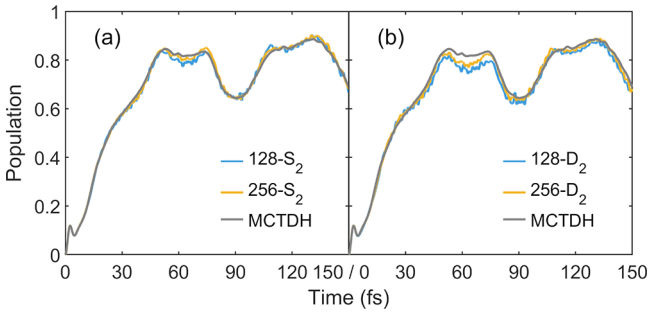

Figure 2. Diabatic population of the $n\pi^*$ state of pyrazine with (a) the multi-S_2 ansatz and (b) the multi-D_2 ansatz. The multiplicity used is $M = 128$ (blue line) and $M = 256$ (yellow line), respectively. For the QVC model, the bilinear parameter $b_{18b,19b}$ is adjusted to the CASSCF value. Both results with the two methods are compared with the MCTDH results (gray lines).

can be seen that the multi-S_2 ansatz provides a better agreement with the MCTDH method. With a multiplicity of $M = 128$, both the multi-S_2 and multi-D_2 ansatz underestimate the population, but it is more obvious for the latter method. An increase in the multiplicity for the multi-S_2 ansatz will reduce the underestimation as a result of $M = 256$ in Figure 2a. On the other hand, although the increasing multiplicity of the multi-D_2 ansatz also reduces the underestimation, a difference can still be clearly recognized at about 60 fs. This shows that the multi-S_2 ansatz is a more appropriate choice for the chemical systems containing quadratic vibronic couplings.

https://doi.org/10.1021/acs.jctc.1c00859
J. Chem. Theory Comput. 2022, 18, 1255−1263

It remains a question of how much additional computational cost would be required with the squeezing operator introduced into the ansatz. Table 1 lists the computational time of the

Table 1. Computational Time of the Full-Modes QVC Model of the Pyrazine via the Multi-S_2 Ansatz, the Multi-D_2 Ansatz, and the MCTDH Method

	S_2 ansatz	D_2 ansatz	MCTDH
M = 128	10.2 h	9.41 h	18.0 h
M = 256	46.3 h	43.7 h	

three methods using 24 CPU cores of Xeon E5-2678. It can be seen that the multi-S_2 ansatz spends 10.2 and 46.3 h for M = 128 and 256 respectively, which is slower than the multi-D_2 ansatz (9.41 and 43.7 h). This is because the multi-S_2 ansatz introduces 24 additional variational parameters, the number of vibrational degrees of freedom. However, the introduced parameters are much fewer than those by only increasing the multiplicity when $\Delta M > 1$. For example, from M = 128 to M = 256, both ansatz will introduce 3328 additional variational parameters. Because both ansatz have the same time complexity (the time complexity of solving linear differential equations), introducing the squeezing operators to the ansatz is affordable to approach the benchmark results for the pyrazine QVC model.

Figure 3 plots the average value of the absolute squeezing parameters within 150 fs with two kinds of the full-modes

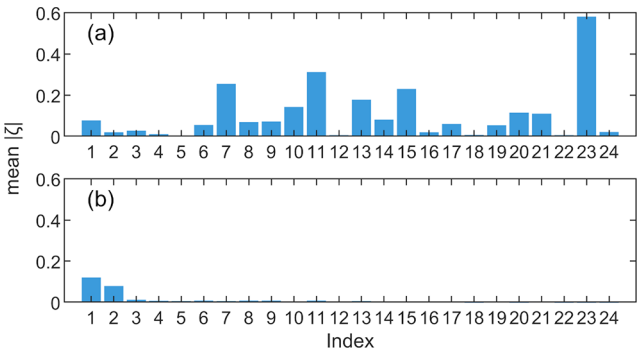

Figure 3. Average absolute squeezing parameters within 150 fs with (a) the full-modes QVC model and (b) the full-modes LVC model. For the QVC model, the bilinear parameter $b_{18b,19b}$ is adjusted to the CASSCF value, and the multiplicity used is M = 128. For the LVC model, the multiplicity used is M = 48.

models, where the multiplicity is M = 128 and 48, respectively. The time evolution is also shown in Figures S1−S4. It can be found that the squeezing parameters are larger and have a more important role for the QVC model, due to the quadratic vibronic couplings. On the other hand, for the LVC model in Figure 3b, there are also nonzero squeezing parameters even without the nonlinear couplings. In Figure 3b and Figures S3 and S4, it can be found that, for the first vibrational mode ν_{10a}, the squeezing parameter is activated in the early stage and has an oscillating motion with the wave function propagating. The squeezing parameter of the second mode ν_{6a} has a little slower activation compared with ν_{10a}. Other vibrational modes exhibit a very small value within the evolutionary time scale, which may be because of the relatively smaller coupling constants.

We then focus on the autocorrelation function and spectroscopy of the QVC model with the same case as that in Figure 2. It is found in Figure 4a that a larger multiplicity leads to a more self-consistent result. For M = 96 and 128, the

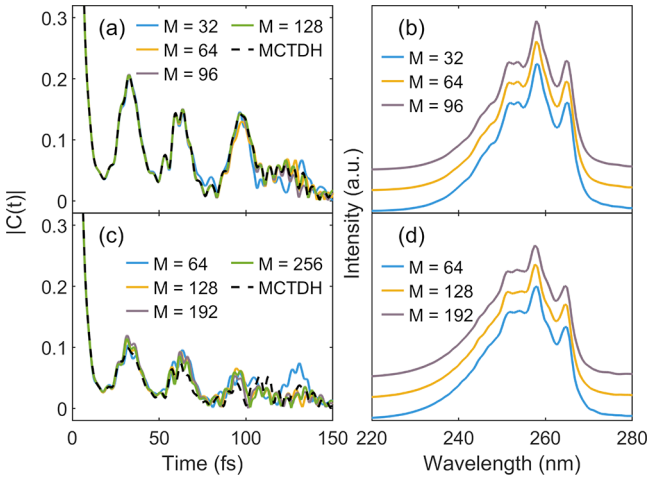

Figure 4. Absolute autocorrelation function and absorption spectrum with (a, b) the reduced QVC model and (c, d) the full-modes QVC model. Solid lines are calculated via the multi-S_2 ansatz with different multiplicities, and dotted lines are the MCTDH results. In the second column, the damping parameter τ is taken as 30 fs for the reduced model and 40 fs for the full-modes model. Each spectrum has been shifted for a clearer comparison.

autocorrelation functions converge in the early stage and slightly differ after about 120 fs. As the multiplicity decreases to 64 and 32, this difference appears earlier at about 90 and 68 fs, respectively. However, when the autocorrelation functions are transformed into the frequency domain to obtain the absorption spectra, all of them show good convergence even for the smallest multiplicity. The absorption spectrum manifests a quicker convergence than the population dynamics and the autocorrelation function, and this feature is also reflected in Figure 4c,d. The autocorrelation function calculated with M = 192 shows good agreement with the counterpart of M = 256, but a slight difference can still be spotted in the latter stage, while smaller multiplicity leads to an earlier difference. With a comparison of the results of the MCTDH method, although the results have good consistency between two methods for the reduced Hamiltonian, there are still differences even with M = 256 for the full-modes one. As the Fourier transformation is applied to the autocorrelation function, the spectra again exhibit a good convergence. Therefore, when using the multi-S_2 ansatz to simulate the spectroscopy, it is tolerant for the multiplicity. On the other hand, if one would like to quantitatively investigate the population dynamics and the autocorrelation function, a larger multiplicity is necessary to obtain reliable results.

Based on the results of Figure 4, finite temperature is taken into account, and the corresponding results are illustrated in Figure 5. First, we focus on the absorption spectrum of the reduced and full-modes QVC model in Figure 5a,b. Herein, the multiplicity is taken as M = 128 for both model Hamiltonians. For the full-modes model, only the four strongest vibrational modes (ν_{6a}, ν_1, ν_{9a}, and ν_{10a}) and others with a frequency smaller than 0.1 eV are adopted into the TFD framework for a more affordable computational cost. It is found that, with increasing temperature, the intensity of the absorption spectrum has a slight decrease but hardly shows

https://doi.org/10.1021/acs.jctc.1c00859
J. Chem. Theory Comput. 2022, 18, 1255−1263

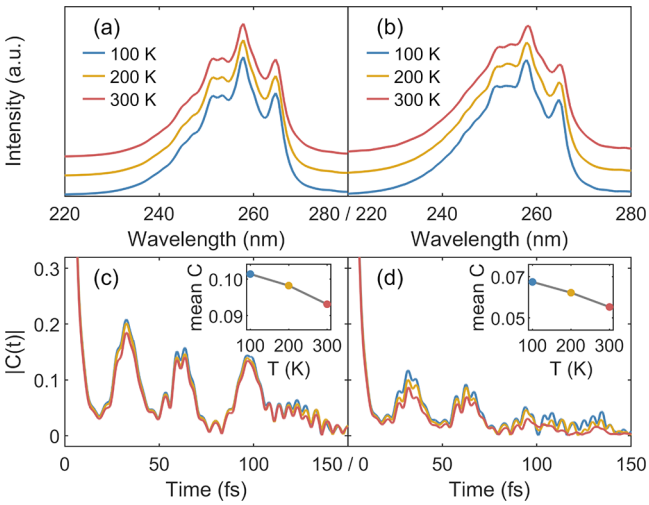

Figure 5. Absorption spectrum with (a) the reduced QVC model and (b) the full-modes QVC model, where the damping parameter τ is taken as 30 and 40 fs, respectively. Each spectrum has been shifted for a clearer comparison. Absolute autocorrelation function with (c) the reduced QVC model and (d) the full-modes QVC model. The inset plots the average value of the absolute autocorrelation function within 150 fs.

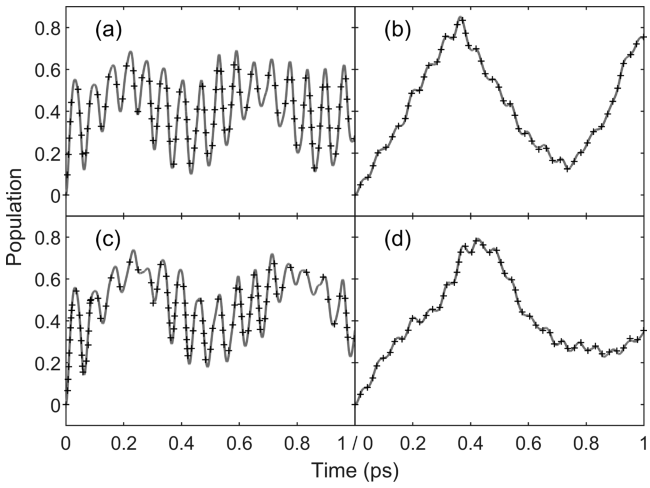

Figure 6. Diabatic population (a) for delocalized excitation with the LVC model, (b) for localized excitation with the LVC model, (c) for delocalized excitation with the QVC model, and (d) for localized excitation with the QVC model. Solid lines are calculated via the multi-S_2 ansatz, and dotted lines are the MCTDH results.[62]

other changes. This is because of the high-frequency vibrational modes reflected as the very small θ_n in the model Hamiltonian, for which phonons are inactive to be excited even at a high temperature. On the other hand, the corresponding autocorrelation function shows similar features in Figure 5c,d. For the reduced model, although the line shape has no changes, a decreasing amplitude is visible as the temperature increases. We average the absolute values within 150 fs and plot them in the inset, showing a decay from 0.1 to 0.093. For the full-modes model, the results have not converged but can provide us a qualitative perspective. As the bathlike vibrational modes are included in the model Hamiltonian, a stronger decay is found from 0.067 to 0.055. Recently, pyrazine has been used for the diradical materials with a triplet ground state.[60] As pyrazine possesses thermal stability, it may be prominent for many applications such as triplet−triplet fluorescence.[61]

3.2. 2-Pyridone Dimer. In the second part, we choose another molecular model 2-pyridone dimer which is abbreviated as $(2PY)_2$. The model Hamiltonian of $(2PY)_2$ was parametrized by Kopec at al.[10] to simulate the vibronic spectroscopy and later used to investigate the excitation transfer behavior by Goswami et al.[62] As the vibrational modes with a high frequency are reduced into the prequenched excitonic splitting, the model can provide a perspective of the influence of those low-frequency ones at zero and finite temperatures, which are relevant to the intermonomeric modes. First, Figure 6 illustrates the reproduced results of the diabatic population for both delocalized and localized excitation within two types of models, namely, LVC and QVC. Herein, for the delocalized excitation, the initial condition is prepared as $B_1(0) = 1$. For the localized excitation, the wave packet propagation is started from $A_1(0) = B_1(0) = \sqrt{2}/2$, and the population is measured with the basis $\sqrt{2}/2(|1\rangle - |2\rangle)$. However, in our simulations, a unitary transformation

$$P = \frac{1}{2}\begin{pmatrix} \sqrt{2} & \sqrt{2} \\ \sqrt{2} & -\sqrt{2} \end{pmatrix} \tag{26}$$

is applied onto both the Hamiltonian

$$H' = PHP^{-1} \tag{27}$$

and the initial condition

$$|S_2'(0)\rangle = P|S_2(0)\rangle \tag{28}$$

for convenience. The multiplicity used is $M = 32$, and the MCTDH results are adopted from ref 62. One can find a good agreement between the results of the multi-S_2 ansatz and the MCTDH method even until a picosecond. It is natural because the Hamiltonian parameters are relatively smaller than in the pyrazine, and thus the simulations are able to converge at a larger time scale. While considering the QVC model in Figure 6c, a stronger dephasing−rephasing crossing can be clearly seen in the quick oscillation, and its second occurrence is deferred to about 0.8 ps compared to the LVC result. This feature is caused by the negative quadratic couplings, which equivalently decrease the vibrational frequencies, leading to the vibronic couplings being stronger and the slow oscillation being slower. A similar phenomenon can be recognized for the localized excitation in Figure 6d.

Having proved the effectiveness, we then take the finite temperature into account. Because vibrational modes with a higher frequency have fewer influences as the temperature increases, the prequenched excitonic splitting can be approximately regarded to have no changes, and the TFD method can be directly employed for the model Hamiltonian. Figures 7 and 8 illustrate the vibronic spectra with the LVC and QVC model, respectively, where the main peak of each line has been normalized and shifted to 0 cm^{-1}. Overall, as the temperature increases, more phonons will be excited, and the relative intensity of the side peaks will be enhanced compared to the main peak. First, we focus on Figure 7. Herein, the multiplicity is taken as $M = 32$, 96, 96, and 128 from 0 to 300 K. When $T > 0$, two peaks at about −10 and −25 cm^{-1} appear which are invisible at zero temperature. The finite temperature also manifests a broadening effect, but even for $T = 300$ K, the

https://doi.org/10.1021/acs.jctc.1c00859
J. Chem. Theory Comput. 2022, 18, 1255−1263

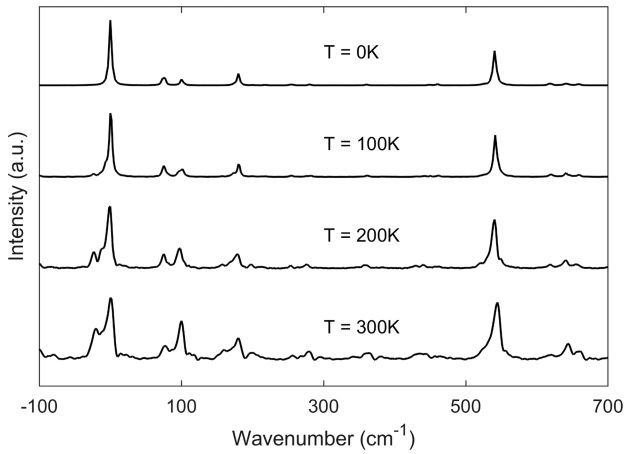

Figure 7. Vibronic spectrum with the LVC model at different temperatures. The damping parameter is taken as τ = 2.5 ps.

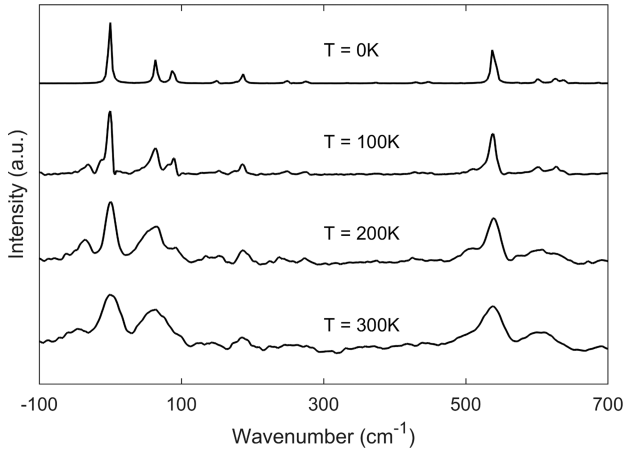

Figure 8. Vibronic spectrum with the QVC model at different temperatures. The damping parameter is taken as τ = 2.5 ps.

side peaks present a good line shape and are well-spotted. However, some of the weak peaks are mixed with the thermal noise, leading to difficult recognitions in practical detections.

The broadening effect can also be found in the simulations of the QVC model but is seen to be much stronger in Figure 8. For T = 100 and 200 K, the side peaks are still distinguishable. As the temperature rises to 300 K, the side peaks are mixed with neighboring peaks and the thermal noise, and only those with a large intensity can be recognized. Similar to the results of the LVC model, the two peaks on the left of the main peak also appear at finite temperature but show an obvious red shift. This effect may be due to the fictitious quadratic couplings and can be utilized as evidence of whether there are strong quadratic couplings in a molecular system, which will be the scope in our future work. Moreover, to obtain the convergent results in Figure 8, the multiplicity is employed with M = 32, 128, 192, and 192 at different T. Due to the negative quadratic couplings and the temperature enhancement with the square of a hyperbolic function, the QVC model is more computationally demanding than the LVC one. A realistic chemical system might involve more complicated interactions such as higher-order vibronic couplings when it comes to a finite temperature. In this case, the effect of the negative quadratic couplings would be suppressed, leading to more affordable computations and less broadening spectra. However, departing from conjecture, the multi-S_2 ansatz has been shown to be able to simulate the vibronic spectroscopy even with such strong quadratic couplings.

In Figure 9a,b, the diabatic populations are depicted with the LVC and QVC model, respectively. In the simulations of the

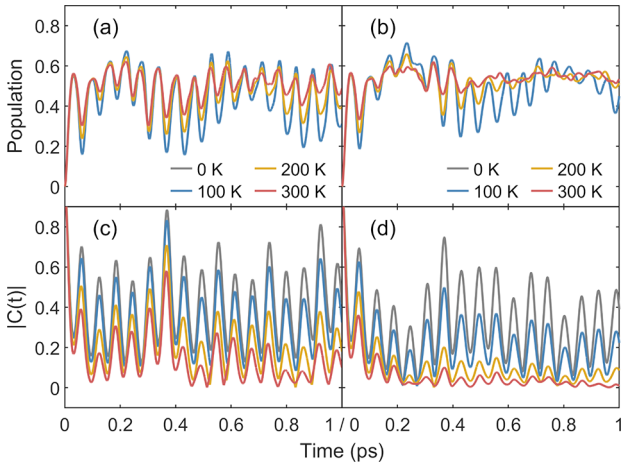

Figure 9. Diabatic population with (a) the LVC model and (b) the QVC model. Absolute autocorrelation function with (c) the LVC model and (d) the QVC model with respect to temperature.

former model, the multiplicity is employed with M = 96, 96, and 128 from 100 to 300 K. Results in the second panel are calculated with M = 128, 512, and 512 with respect to the temperature. However, it should be mentioned that the QVC results have still not converged at T = 200 (after about 700 fs) and 300 K (after about 500 fs). Both sets of the results show that the temperature effect begins to influence the system after about 60 fs, which is relevant to the vibrational modes ν_{15} and ν_{16}.[62] With T increasing, the population experiences stronger damping as the oscillation is weakened, which is seen to be more obvious for the QVC results. When the temperature rises to 300 K, both the LVC and QVC populations approach their thermal equilibrium. Furthermore, we also show the corresponding autocorrelation function in Figure 9c,d. Herein, zero-temperature results with the same condition as in Figure 6a,c are also depicted. When T = 0, the system maintains a good feature of coherence which oscillates around 0.4 and 0.3, respectively. The finite temperature begins to affect the autocorrelation function earlier than the populations and leads to a decoherence effect. This feature is stronger at a long time scale. For the two types of models, a temperature up to 300 K finally makes the autocorrelation function decay to nearly zero. In addition, from a computational viewpoint, although the multiplicity employed is same as the case of the diabatic population, a better convergence is found for the autocorrelation function of the QVC model at T = 200 and 300 K. This is because eq 25 uses the wave function at time $t/2$ rather than t. However, it also requires a larger multiplicity compared to the vibronic spectroscopy.

4. CONCLUSION

By introducing the squeezing operator into the multiple Davydov ansatz, we proposed the so-called multi-S_2 ansatz for an accurate dynamics simulation in the presence of nonlinear vibronic couplings. Two realistic chemical systems, the pyrazine and the $(2PY)_2$, were calculated to exhibit its

https://doi.org/10.1021/acs.jctc.1c00859
J. Chem. Theory Comput. 2022, 18, 1255−1263

efficiency and accuracy. The results suggest that the multi-S_2 ansatz is able to provide reliable simulations for both the LVC and QVC models, which are in agreement with the diabatic population of the MCTDH method. It is found that the population and the autocorrelation function are more demanding on the multiplicity. However, while focusing on the spectroscopy, a small multiplicity is adequate to obtain the convergent result. The finite temperature was also taken into consideration thanks to the TFD method. For the pyrazine, due to the high-frequency vibrational modes of the system, the absorption spectrum and the autocorrelation function manifest thermal stability as the temperature increases. On the other hand, the temperature effect is more influential for the $(2PY)_2$ because of the low vibrational frequencies. Besides intensifying and broadening the vibronic spectrum, the finite temperature is relevant to the side peaks on the left of the main peak and leads to a red shift effect for the QVC model, which might be evidence of the quadratic couplings in the vibronic spectroscopy. In addition, the finite temperature will give rise to a damping effect and decoherence in the population and the autocorrelation function, which become stronger while involving the quadratic couplings in the system.

■ ASSOCIATED CONTENT

Supporting Information

The Supporting Information is available free of charge at https://pubs.acs.org/doi/10.1021/acs.jctc.1c00859.

Computational results and derivation details, including time evolution of the squeezing parameters of the full-modes pyrazine model, equations of motion of the multi-S_2 ansatz, and expressions of the calculated observables (PDF)

■ AUTHOR INFORMATION

Corresponding Author

Yao Yao − *Department of Physics, South China University of Technology, Guangzhou 510640, China; State Key Laboratory of Luminescent Materials and Devices, South China University of Technology, Guangzhou 510640, China;* Email: yaoyao2016@scut.edu.cn

Author

Jiarui Zeng − *Department of Physics, South China University of Technology, Guangzhou 510640, China;* orcid.org/0000-0002-5420-3765

Complete contact information is available at: https://pubs.acs.org/10.1021/acs.jctc.1c00859

Notes

The authors declare no competing financial interest.

■ ACKNOWLEDGMENTS

This work was supported by the Key Research and Development Project of Guangdong Province (Grant 2020B0303300001), the National Natural Science Foundation of China (Grants 91833305 and 11974118), the Guangdong−Hong Kong−Macao Joint Laboratory of Optoelectronic and Magnetic Functional Materials program (2019B121205002), and the Fundamental Research Funds for the Central Universities (Grant 2019ZD51). We gratefully acknowledge G. A. Worth, M. H. Beck, A. Jäckle, and H.-D. Meyer for the Heidelberg MCTDH program package.

■ REFERENCES

(1) Köppel, H.; Domcke, W.; Cederbaum, L. S. Multimode Molecular Dynamics beyond the Born-Oppenheimer Approximation. In *Advances in Chemical Physics*; Wiley, 1984.; Vol. *57*, pp 59−246.

(2) Born, M.; Oppenheimer, R. Zur Quantentheorie der Molekeln. *Ann. Phys.* **1927**, *389*, 457−484.

(3) Yarkony, D. R. Current Issues in Nonadiabatic Chemistry. *J. Phys. Chem.* **1996**, *100*, 18612−18628.

(4) Sun, K.; Xu, Q.; Chen, L.; Gelin, M. F.; Zhao, Y. Temperature Effects on Singlet Fission Dynamics Mediated by a Conical Intersection. *J. Chem. Phys.* **2020**, *153*, 194106.

(5) Kondo, Y.; Yoshiura, K.; Kitera, S.; Nishi, H.; Oda, S.; Gotoh, H.; Sasada, Y.; Yanai, M.; Hatakeyama, T. Narrowband Deep-Blue Organic Light-Emitting Diode Featuring an Organoboron-Based Emitter. Nat. *Photonics* **2019**, *13*, 678−682.

(6) Thiel, A.; Köppel, H. Proposal and Numerical Test of a Simple Diabatization Scheme. *J. Chem. Phys.* **1999**, *110*, 9371−9383.

(7) Worth, G. A.; Meyer, H.-D.; Cederbaum, L. The Effect of a Model Environment on the S_2 Absorption Spectrum of Pyrazine: A Wave Packet Study Treating All 24 Vibrational Modes. *J. Chem. Phys.* **1996**, *105*, 4412−4426.

(8) Raab, A.; Worth, G. A.; Meyer, H.-D.; Cederbaum, L. Molecular Dynamics of Pyrazine after Excitation to the S_2 Electronic State Using a Realistic 24-Mode Model Hamiltonian. *J. Chem. Phys.* **1999**, *110*, 936−946.

(9) Kopec, S.; Ottiger, P.; Leutwyler, S.; Köppel, H. Analysis of the $S_2 \leftarrow S_0$ Vibronic Spectrum of the Ortho-Cyanophenol Dimer Using a Multimode Vibronic Coupling approach. *J. Chem. Phys.* **2015**, *142*, 084308.

(10) Kopec, S.; Köppel, H. Theoretical Analysis of the $S_2 \leftarrow S_0$ Vibronic Spectrum of the 2-Pyridone Dimer. *J. Chem. Phys.* **2016**, *144*, 024314.

(11) Worth, G. A.; Cederbaum, L. S. Beyond Born-Oppenheimer: Molecular Dynamics through a Conical Intersection. *Annu. Rev. Phys. Chem.* **2004**, *55*, 127−158.

(12) Domcke, W.; Yarkony, D. R. Role of Conical Intersections in Molecular Spectroscopy and Photoinduced Chemical Dynamics. *Annu. Rev. Phys. Chem.* **2012**, *63*, 325−352.

(13) Picconi, D.; Lami, A.; Santoro, F. Hierarchical Transformation of Hamiltonians with Linear and Quadratic Couplings for Non-adiabatic Quantum Dynamics: Application to the $\pi\pi^*/n\pi^*$ Internal Conversion in Thymine. *J. Chem. Phys.* **2012**, *136*, 244104.

(14) Ghosh, A.; Rajak, K.; Kanakati, A. K.; Mahapatra, S. Renner-Teller and Pseudo-Renner-Teller Interactions in the Electronic Ground and Excited States of the Dicyanoacetylene Radical Cation: Assignment of Vibronic Spectrum and Elucidation of Nonradiative and Radiative Decay Mechanisms. *Comput. Theor. Chem.* **2019**, *1155*, 109−124.

(15) Grossmann, F. *Theoretical Femtosecond Physics: Atoms and Molecules in Strong Laser Fields*; Springer, 2018.

(16) Beck, M. H.; Jäckle, A.; Worth, G. A.; Meyer, H.-D. The Multiconfiguration Time-Dependent Hartree (MCTDH) Method: A Highly Efficient Algorithm for Propagating Wavepackets. *Phys. Rep.* **2000**, *324*, 1−105.

(17) Meyer, H.-D.; Manthe, U.; Cederbaum, L. S. The Multi-Configurational Time-Dependent Hartree Approach. *Chem. Phys. Lett.* **1990**, *165*, 73−78.

(18) Manthe, U.; Meyer, H.-D.; Cederbaum, L. S. Wave-Packet Dynamics within the Multiconfiguration Hartree Framework: General Aspects and Application to NOCl. *J. Chem. Phys.* **1992**, *97*, 3199−3213.

(19) Wang, H.; Thoss, M. Multilayer Formulation of the Multiconfiguration Time-Dependent Hartree Theory. *J. Chem. Phys.* **2003**, *119*, 1289−1299.

(20) Schollwöck, U. The Density-Matrix Renormalization Group. *Rev. Mod. Phys.* **2005**, *77*, 259−315.

(21) Yao, Y.; Sun, K.-W.; Luo, Z.; Ma, H. Full Quantum Dynamics Simulation of a Realistic Molecular System Using the Adaptive Time-

Dependent Density Matrix Renormalization Group Method. *J. Phys. Chem. Lett.* **2018**, *9*, 413−419.
(22) Xie, X.; Liu, Y.; Yao, Y.; Schollwöck, U.; Liu, C.; Ma, H. Time-Dependent Density Matrix Renormalization Group Quantum Dynamics for Realistic Chemical Systems. *J. Chem. Phys.* **2019**, *151*, 224101.
(23) White, S. R. Density Matrix Formulation for Quantum Renormalization Groups. *Phys. Rev. Lett.* **1992**, *69*, 2863.
(24) Kühl, A.; Domcke, W. Multilevel Redfield Description of the Dissipative Dynamics at Conical Intersections. *J. Chem. Phys.* **2002**, *116*, 263−274.
(25) Tanimura, Y.; Kubo, R. Time Evolution of a Quantum System in Contact with a Nearly Gaussian-Markoffian Noise Bath. *J. Phys. Soc. Jpn.* **1989**, *58*, 101−114.
(26) Tanimura, Y. Numerically "Exact" Approach to Open Quantum Dynamics: The Hierarchical Equations of Motion (HEOM). *J. Chem. Phys.* **2020**, *153*, 020901.
(27) Werther, M.; Choudhury, S. L.; Großmann, F. Coherent State Based Solutions of the Time-Dependent Schrödinger Equation: Hierarchy of Approximations to the Variational Principle. *Int. Rev. Phys. Chem.* **2021**, *40*, 81−125.
(28) Tanaka, S. Ultrafast Relaxation Dynamics of the One-Dimensional Molecular Chain: The Time-Resolved Spontaneous Emission and Exciton Coherence. *J. Chem. Phys.* **2003**, *119*, 4891−4904.
(29) Wu, N.; Duan, L.; Li, X.; Zhao, Y. Dynamics of the Sub-Ohmic Spin-Boson Model: A Time-Dependent Variational Study. *J. Chem. Phys.* **2013**, *138*, 084111.
(30) Sun, K.-W.; Yao, Y. Beating Maps of Singlet Fission: Simulation of Coherent Two-Dimensional Electronic Spectroscopy by Davydov Ansatz in Organic Molecules. *J. Chem. Phys.* **2017**, *147*, 224905.
(31) Werther, M.; Grossmann, F. The Davydov D1.5 Ansatz for the Quantum Rabi Model. Phys. *Scripta* **2018**, *93*, 074001.
(32) Chen, L.; Gelin, M.; Zhao, Y. Dynamics of the Spin-Boson Model: A Comparison of the Multiple Davydov D_1, $D_{1.5}$, D_2 Ansätze. *Chem. Phys.* **2018**, *515*, 108−118.
(33) Grossmann, F.; Werther, M.; Chen, L.; Zhao, Y. Generalization of the Davydov Ansatz by Squeezing. *Chem. Phys.* **2016**, *481*, 99−107.
(34) Chorošajev, V.; Marčiulionis, T.; Abramavicius, D. Temporal Dynamics of Excitonic States with Nonlinear Electron-Vibrational Coupling. *J. Chem. Phys.* **2017**, *147*, 074114.
(35) Abramavičius, D.; Marčiulionis, T. Excitation Dynamics of Two Level Quantum Systems Coupled to Morse Vibrations. *Lith. J. Phys.* **2019**, *58*, 3875.
(36) Adhikari, S.; Billing, G. D. The Hermite Correction Method for Nonadiabatic Transitions. *J. Chem. Phys.* **1999**, *111*, 48−53.
(37) Billing, G. D. Quantum Dressed Classical Mechanics: Application to Non-Adiabatic Processes. *Chem. Phys. Lett.* **2001**, *343*, 130−138.
(38) Billing, G. Quantum-Dressed Classical Mechanics: Theory and Application. *Phys. Chem. Chem. Phys.* **2002**, *4*, 2865−2877.
(39) Coletti, C.; Billing, G. D. Quantum Dressed Classical Mechanics: Application to the Photo-Absorption of Pyrazine. *Chem. Phys. Lett.* **2003**, *368*, 289−298.
(40) Borrelli, R.; Peluso, A. Quantum Dynamics of Electronic Transitions with Gauss-Hermite Wave Packets. *J. Chem. Phys.* **2016**, *144*, 114102.
(41) Borrelli, R.; Gelin, M. F. The Generalized Coherent State ansatz: Application to quantum electron-vibrational dynamics. *Chem. Phys.* **2016**, *481*, 91−98.
(42) Chen, L.; Borrelli, R.; Zhao, Y. Dynamics of Coupled Electron−Boson Systems with the Multiple Davydov D_1 Ansatz and the Generalized Coherent State. *J. Phys. Chem. A* **2017**, *121*, 8757−8770.
(43) Zhou, N.; Huang, Z.; Zhu, J.; Chernyak, V.; Zhao, Y. Polaron dynamics with a multitude of Davydov D2 trial states. *J. Chem. Phys.* **2015**, *143*, 014113.
(44) Wang, L.; Chen, L.; Zhou, N.; Zhao, Y. Variational dynamics of the sub-Ohmic spin-boson model on the basis of multiple Davydov D1 states. *J. Chem. Phys.* **2016**, *144*, 024101.
(45) Chen, L.; Gelin, M. F.; Domcke, W. Multimode Quantum Dynamics with Multiple Davydov D_2 Trial States: Application to a 24-Dimensional Conical Intersection Model. *J. Chem. Phys.* **2019**, *150*, 024101.
(46) Sun, K.; Huang, Z.; Gelin, M. F.; Chen, L.; Zhao, Y. Monitoring of Singlet Fission via Two-Dimensional Photon-Echo and Transient-Absorption Spectroscopy: Simulations by Multiple Davydov Trial States. *J. Chem. Phys.* **2019**, *151*, 114102.
(47) Takahashi, Y.; Umezawa, H. Thermo Field Dynamics. *Int. J. Mod. Phys. B* **1996**, *10*, 1755−1805.
(48) Gelin, M. F.; Borrelli, R. Thermal Schrödinger Equation: Efficient Tool for Simulation of Many-Body Quantum Dynamics at Finite Temperature. *Ann. Phys.* **2017**, *529*, 1700200.
(49) Borrelli, R.; Gelin, M. F. Quantum Electron-Vibrational Dynamics at Finite Temperature: Thermo Field Dynamics Approach. *J. Chem. Phys.* **2016**, *145*, 224101.
(50) Borrelli, R.; Gelin, M. F. Simulation of Quantum Dynamics of Excitonic Systems at Finite Temperature: An Efficient Method Based on Thermo Field Dynamics. *Sci. Rep.* **2017**, *7*, 1−9.
(51) Borrelli, R. Theoretical Study of Charge-Transfer Processes at Finite Temperature Using a Novel Thermal Schrödinger Equation. *Chem. Phys.* **2018**, *515*, 236−241.
(52) Borrelli, R.; Gelin, M. F. Finite Temperature Quantum Dynamics of Complex Systems: Integrating Thermo-Field Theories and Tensor-Train Methods. *WIREs Comput. Mol. Sci.* **2021**, *11*, No. e1539.
(53) Gelin, M. F.; Borrelli, R. Simulation of Nonlinear Femtosecond Signals at Finite Temperature via a Thermo Field Dynamics-Tensor Train Method: General Theory and Application to Time-and Frequency-Resolved Fluorescence of the Fenna−Matthews−Olson Complex. *J. Chem. Theory Comput.* **2021**, *17*, 4316.
(54) Gelin, M. F.; Velardo, A.; Borrelli, R. Efficient Quantum Dynamics Simulations of Complex Molecular Systems: A Unified Treatment of Dynamic and Static Disorder. *J. Chem. Phys.* **2021**, *155*, 134102.
(55) Chen, L.; Zhao, Y. Finite Temperature Dynamics of a Holstein Polaron: The Thermo-Field Dynamics Approach. *J. Chem. Phys.* **2017**, *147*, 214102.
(56) Fisher, R. A.; Nieto, M. M.; Sandberg, V. D. Impossibility of Naively Generalizing Squeezed Coherent States. *Phys. Rev. D* **1984**, *29*, 1107.
(57) Puzari, P.; Sarkar, B.; Adhikari, S. A Quantum-Classical Approach to the Molecular Dynamics of Pyrazine with a Realistic Model Hamiltonian. *J. Chem. Phys.* **2006**, *125*, 194316.
(58) Saller, M. A.; Habershon, S. Basis Set Generation for Quantum Dynamics Simulations Using Simple Trajectory-Based Methods. *J. Chem. Theory Comput.* **2015**, *11*, 8−16.
(59) Worth, G. A.; Beck, M. H.; Jäckle, A.; Meyer, H.-D. *The MCTDH Package*, Version 8.2, (2000). H.-D. Meyer, Version 8.3 (2002), Version 8.4 (2007). Used version: 8.4.20 (2020). See http://mctdh.uni-hd.de.
(60) Wang, Z.-Y.; Dai, Y.-Z.; Ding, L.; Dong, B.-W.; Jiang, S.-D.; Wang, J.-Y.; Pei, J. A Stable Triplet-Ground-State Conjugated Diradical Based on a Diindenopyrazine Skeleton. *Angew. Chem., Int. Ed.* **2021**, *60*, 4594−4598.
(61) Namai, H.; Ikeda, H.; Hoshi, Y.; Kato, N.; Morishita, Y.; Mizuno, K. Thermoluminescence and a New Organic Light-Emitting Diode (OLED) Based on Triplet-Triplet Fluorescence of the Trimethylenemethane (TMM) Biradical. *J. Am. Chem. Soc.* **2007**, *129*, 9032−9036.
(62) Goswami, S.; Kopec, S.; Köppel, H. Vibronic Coupling and Excitation Transfer in Hydrogen-Bonded Molecular Dimers: A Quantum Dynamical Analysis. *J. Phys. Chem. A* **2019**, *123*, 5491−5503.

https://doi.org/10.1021/acs.jctc.1c00859
J. Chem. Theory Comput. 2022, 18, 1255−1263